

# Assign and Add: A Mechanistic Study of Compositional Arithmetic

Brady Exoo  
Yale University

Alberto Bietti  
Flatiron Institute

John Sous  
Yale University

June 1, 2026

## Abstract

Large language models are able to compose skills in order to perform complex tasks, many of which might not have been seen during training. The details of how exactly this composition occurs remain elusive. In this paper, we study a mechanism for compositional generalization in transformers by considering a simple controlled setting involving variable assignment and modular addition. By partitioning our training data into disjoint sets, we observe that small transformers are able to generalize to previously unseen combinations of variables and numbers. Our mechanistic analysis shows that the same “modular addition” MLP module is used whether the inputs are given directly or indirectly through a separate variable assignment mechanism. We also analyze the training dynamics from an empirical lens, which reveals three phases of learning: first, modular addition is learned, then the structure required for variable assignment, and finally a refinement phase where the model generalizes to some hard sequences not seen in training. Finally, we provide a theoretical framework to explain how compositionality emerges from training dynamics. These results suggest that compositional generalization can be a natural consequence of the compositionality of internal mechanisms in transformers.

## 1 Introduction

The reliability of large language models on reasoning tasks depends critically on their ability to generalize across variations of problems they might have seen during training. A central mechanism for their ability (or failure) to generalize is *compositionality* [1–4]: tackling complex tasks as a composition of small atomic mechanisms provides a reliable way to generalize, similar to how a small valid program is guaranteed to work on arbitrary inputs. While the generalization capabilities of modern LLMs are improving, a deeper understanding of how they learn to generalize via composition is still missing, and could further improve their reliability. . Studying mechanisms in transformers and their training dynamics in controlled settings via mechanistic interpretability provides a framework for understanding how these generalizing capabilities arise in transformers. Our goal in this paper is to systematically study how training a transformer on a simple compositional task may lead to compositionality of the mechanisms in its architecture, and how this enables out-of-distribution generalization. Specifically, we take two well-studied mechanisms with highly different behaviors—variable binding and modular addition—and consider a task involving their composition. Variable binding often relies on an induction head circuit [5, 6], which implements an associative recall mechanism, a fundamental operation even in large models which has been well-studied from a training dynamics standpoint using associative memories [7–9]. Modular arithmetic is a mathematical task which typically leads to highly structured representations involving Fourier features, and often exhibits “grokking” in its training dynamics — a phenomenon where a model initially overfits and memorizes the training data before eventually transitioning to generalizable reasoning [10–13]. Since mathematical reasoning in scientific domains often combines information retrieval with arithmetic operations, this raises the following questions:

*How do transformers learn to compose variable binding and modular addition mechanisms to generalize beyond the training distribution? How do these capabilities emerge during training?*

In this paper, we study these questions in a controlled setting, revealing how transformers learn to compose variable binding with arithmetic ability. Specifically, we analyze a 2-layer transformer trained to perform modular addition where the operands may be variables that were dynamically assigned in the context.

Our main contributions are as follows:

- We present a tractable model for mechanistically interpreting compositional arithmetic induced by composing variable assignment with modular arithmetic.
- We analyze the training dynamics, revealing that modular arithmetic is learned prior to and independently of variable assignment. We find that the model attains near-perfect test accuracy on 0-variable modular addition while still learning to perform variable assignment.
- We provide a thorough mechanistic study of the model at the end of training, and show that generalization arises via composition of the modular addition circuit, implemented by the last MLP, and a modified induction head circuit, whereby the second layer attends to the numbers assigned to the correct variables involved in the addition.
- We provide a theoretical analysis of how gradient dynamics allow the composition of the variable binding and modular addition circuits.

**Related work.** The problem of composition in mechanistic interpretability has been studied on pretrained models via circuit analysis [e.g., 14–16], as well as on small transformers in synthetic controlled settings involving, e.g., variable binding, state tracking, arithmetic, or in-context learning [11, 17–23]. Compared to these works, our focus is on how composition arises during training in a controlled setting, and on a detailed understanding—at the weights level—of the composition of two very different types of mechanisms (associative recall via induction heads and modular addition via non-linear Fourier features), backed by a theoretical analysis of gradient dynamics. Induction heads were introduced and analyzed empirically in [5, 6], after which theoretical work revealed that optimization dynamics implements associative memory through the induction head mechanism [7, 24]. This connection between associative memory and induction heads has received interest in the context of solving recursions [25]. Grokking was first discovered in the context of small algorithmic datasets [10]. Later, mechanistic models based on one or few layer architectures have revealed the emergence of Fourier features in the grokking learning process [11, 12], and recent works have studied their training dynamics theoretically [13, 26, 27]. Ref. [28] studies training dynamics on a compositional multi-hop reasoning task, but their theoretical setup is idealized and not directly related to mechanistic analysis of a generically trained model.

## 2 Background

This section reviews preliminaries on the main concepts we use in this work.

**Transformer architecture.** Our architecture utilizes a 2-layer, single-head transformer that deliberately omits the layer-1 MLP. A single-head transformer [29] maps each token in a vocabulary of  $n$  discrete tokens to a  $d_{\text{model}}$ -dimensional vector via the embedding matrix  $W_E$ . For a detailed exposition of the transformer architecture from a mechanistic-interpretability perspective, see Elhage et al. [5]. Following the mechanistic interpretability framework established in [5], we conceptually separate the operations of each attention head into two distinct linear circuits. The Query-Key (QK) circuit, characterized by the weight matrices  $W_Q$  and  $W_K$ , computes the attention pattern matrix and determines where information is routed across the sequence. Simply put, it calculates how much the current token should “listen to” or draw information from each of the preceding tokens. The Output-Value (OV) circuit, characterized by  $W_V$  and  $W_O$ , determines what information is extracted from the source token and written into the destination token’s residual stream. Following an attention layer, the residual stream is typically passed through an MLP, which operates on each token position independently to compute non-linear transformations. Therefore, in our architecture, the residual stream only undergoes this non-linear MLP transformation following the second attention layer. Once the sequence has been processed through all attention and MLP sublayers, the unembedding matrix,  $W_U$ , linearly projects the final residual stream vector of the last token back into the vocabulary space to yield the output logits. A softmax transformation is applied to normalize the logits, and the model’s final prediction is the argmax of the normalized logits.

**Induction head mechanisms and associative memories.** Induction heads are a common mechanism found in transformers with at least 2 attention layers that support in-context learning [6]. Generally,

PAD	PAD	PAD	PAD	c	1	PAD	f	17	a	42	PAD	+	f	19	=	36
b	2	PAD	g	08	PAD	c	53	PAD	PAD	e	14	+	17	32	=	49
a	3	c	58	PAD	d	19	f	06	b	47	PAD	+	b	f	=	53

Figure 1: Examples of tokenized sequences formed of variables and constants. The final token in blue represents the target answer, and is not present in the training sequence. Note that the third sequence will be in the test set, since it has  $b$  in the first position of the addition.

these heads implement a copying mechanism that takes inputs of the form  $[\dots A B \dots A]$  and predicts  $B$ . In our model, rather than copying a token, we find a modified induction-head mechanism that retrieves assigned variables and routes their assigned values into the downstream MLP to compute modular addition. Following [7, 30], our mechanistic analysis leverages the view of attention matrices as associative memories that capture associations between pairs of embeddings, leading to specific attention behaviors.

**Modular addition with Fourier features.** Our analysis leverages the findings of previous literature on modular addition, namely that neural networks tend to learn structured Fourier representations to solve this task. This is typically done with input and output weights of an MLP that are sinusoidal, in a way that summing neurons for a given label yields constructive interference [12]. Such a generalizing solution often appears after an initial memorization phase, a typical example of grokking.

### 3 Setup

This section presents the data distribution and model architecture we utilize, with the goal of designing a task that requires composition of at least two different mechanisms (specifically, modular addition and variable binding), while remaining tractable to analyze mechanistically. Our code is available at [MechCompose](#).

**Model.** We train a 2-layer transformer with a single attention head,  $d_{\text{model}} = d_{\text{head}} = 128$ , and  $d_{\text{mlp}} = 512$ , using GPT-2-style absolute positional embeddings [31], implemented in TransformerLens [32], an open-source library for mechanistic interpretability released under the MIT License. To simplify circuit discovery, we omit biases and normalization layers. We also remove the layer-1 MLP, as we find it unnecessary to perform the task. We implement attention using causal masking. Our model is trained with AdamW [33] using a learning rate of  $10^{-3}$  and weight decay of  $2 \times 10^{-2}$ . While our mechanistic analysis focuses on a single training run, we expect our findings to hold across different initializations.

**Data distribution.** We consider a problem of variable assignment and modular addition, with sequences such as  $c=1, b=17, a=42, b+19=?$ , where addition is performed modulo  $N = 59$  over  $V = 12$  distinct variables. Each sequence of size  $T = 16$  is tokenized as shown in Figure 1, with random padding added to prevent solutions that rely explicitly on absolute position. Note also that our tokenization omits  $=$  in the variable assignments and the  $?$  at the end of the sequence, and represents addition in a modified order: due to causal masking, we place the  $+$  token before the operands to signal the start of the addition operation.

To evaluate the model’s ability to generalize, we remove approximately 30% of the  $59^2$  possible addition pairs from the training data. Concretely, if  $(1, 3)$  is removed from the training set, then all sequences containing  $1+3$ ;  $c=1, c+3$ ; and  $c=3, 1+c$  are also removed. We also constrain certain variables to fixed positions in the addition. In particular, in the training set the variables  $a$  and  $b$  are restricted from appearing in the first position of the addition (position 13 of the sequence) and  $g$  and  $h$  are restricted from appearing in the last position of the addition (position 14 of the sequence).

Let  $S$  denote the set of all valid sequences. We partition  $S$  into  $S_0, S_1$ , and  $S_2$ , the sets of sequences in which the addition contains 0, 1, and 2 variables, respectively. We also partition  $S$  according to the restrictions imposed on the training set. Let  $S_V$  be the set of sequences in which variables appear only in valid positions, and let  $S_A$  be the set of sequences with valid addition constant pairs. Our training set is then  $S_T = S_V \cap S_A$ . Finally, we generate sequences satisfying these constraints on-the-fly during training, rather than pre-partitioning a fixed set of sequences into training and test splits.

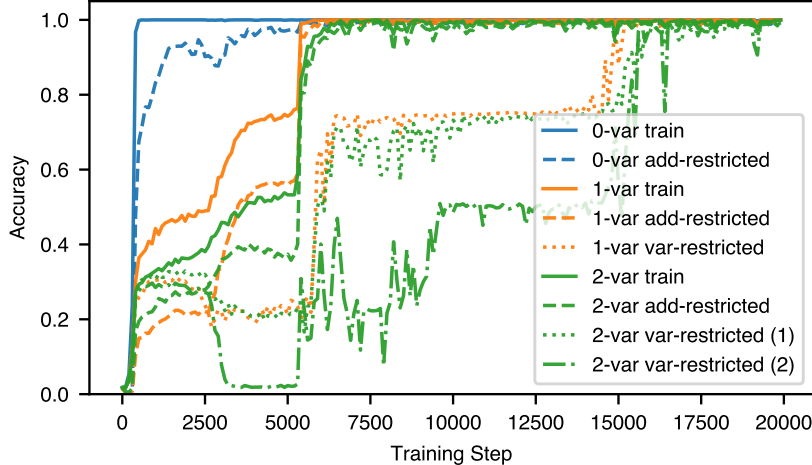


Figure 2: **Accuracies during training partitioned by evaluation set.** Add-restricted sets contain sequences with held-out addition pairs as discussed in Section 3, and var-restricted sets contain sequences with held-out variable positions. The (1) and (2) for the 2-var var-restricted sets denote how many of the variables are in “bad” positions. Train sets are those with both valid addition pairs and variable positions. An alternate run is displayed in Appendix A Figure 10.

In what follows, we analyze our results with respect to 0-variable (0-var), 1-variable (1-var), and 2-variable (2-var) tasks.

## 4 Generalization Results

We first describe several ways in which our model generalizes.

**Training results.** In Figure 2, our model achieves over 98% test accuracy across all addition types (0-var, 1-var, and 2-var). We find that learning proceeds in distinct phases: the model first learns to perform addition on sequences with no variable operands (0-var addition), and only later learns variable–constant and variable–variable addition. In Section 6, we analyze this behavior in more detail. Notably, the model learns to generalize to sequences with novel variable positions. For example, after learning from  $b=17$  and  $14+b=31$ , the model can correctly predict the previously unseen ordering  $b+14$  and produce 31. On a curated test set consisting specifically of such cases, the model achieves 99.6% accuracy. Moreover, although training omits specific modular additions—for example, a dataset may contain no instance of  $1+3$  in any form, including  $1+3$ ,  $c=1$ ,  $c+3$ , and  $c=3$ ,  $1+c$ —the model nevertheless learns to predict these held-out cases. Similarly, on a curated test set consisting specifically of such latter cases, the model achieves 99.4% accuracy.

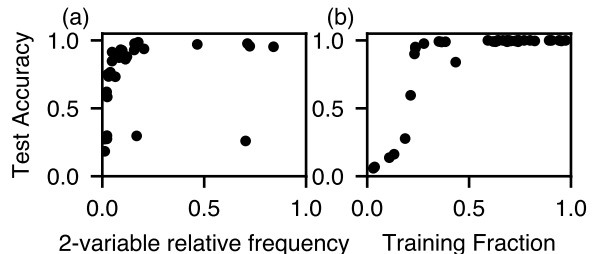


Figure 3: **Data requirements for generalization.** (a) Test accuracy on 2-variable sequences as a function of their relative frequency in the training set. The model requires a relative frequency of  $r \approx 0.2$  to successfully generalize. (b) Test accuracy on 0-variable sequences as a function of the fraction of all possible addition pairs seen during training. Generalization to unseen constant pairs requires training on at least  $f \approx 0.25$  of the total distribution.

**Training set pairs.** We train multiple models using different fractions  $f \in (0, 1)$  of the  $59^2$  addition pairs in the training set. Figure 3 shows the zero-variable test accuracy after 30000 training steps as a function of

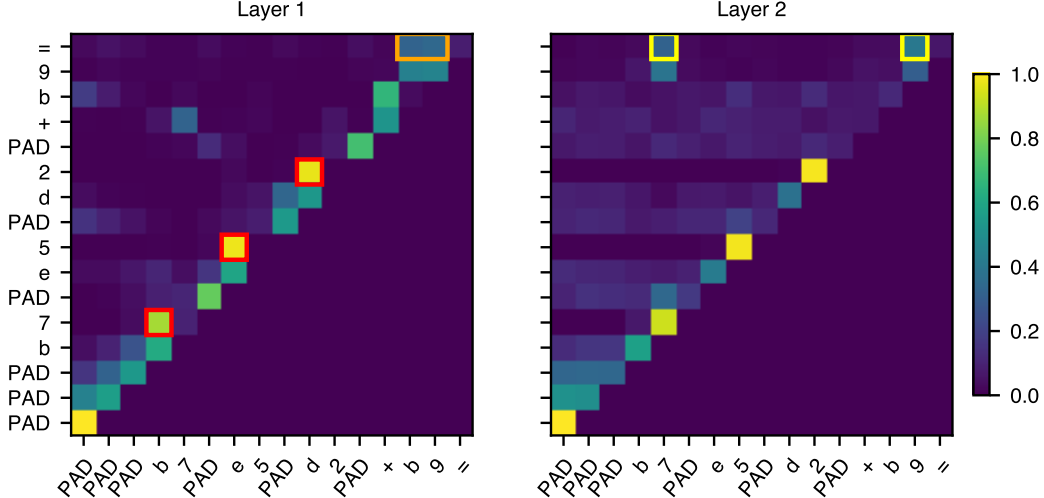


Figure 4: **Attention patterns for an example sequence. Left (Layer 1):** The = token attends to the two immediately preceding positions representing the operands (orange boxes). Simultaneously, constant tokens in positions 1–11 act as previous-token heads, attending to their assigned variables (red boxes). **Right (Layer 2):** The = token attends directly to the constants required for the addition (yellow boxes). These behaviors are consistent across all sequences and training initializations.

the fraction of addition pairs included in training. We observe we need at least  $f \gtrsim 0.25$  in order to generalize to the entire 0-var set.

**Two-variable priming** We train multiple models with different relative frequencies  $r \in (0, 1]$  as the ratio of the number of two-variable addition sequences to the number of zero-variable sequences in the training set. Figure 3 displays the two-variable test accuracy after 30000 training steps. We observe  $r \gtrsim 0.2$  is required for the model to generalize to all 2-variable sequences.

## 5 Emergent Mechanisms and Compositionality

In this section, we analyze the model’s internals at the end of training to empirically derive the mechanism driving generalization via composition.

We first analyze the attention patterns for an exemplary sequence in Figure 4. In the second attention layer, the final = token—the position responsible for outputting the result—attends strongly to the specific operands required for the computation (e.g., 7 and 9 in the figure). This targeted attention implies that the modular addition itself is computed downstream of the query-key circuit, specifically via the combination of the layer-2 output-value (OV) matrix and the layer-2 MLP.

Next, we isolate the OV-MLP circuit from the query-key routing to demonstrate how these components decouple in order to compute modular addition with or without variables.

### 5.1 Modular addition with the OV-MLP Circuit

To confirm the above intuition that the modular addition circuit happens downstream of the layer 2 query-key matrix, we analyze the residual stream vector at the = token immediately preceding the layer-2 MLP. Let  $a$  and  $b$  denote the raw token embeddings of the two target constants that are being added. In Figure 5 we compute the cosine similarity between the pre-MLP residual vector and the sum of their independent layer-2 output-value projections,  $OV_2(a) + OV_2(b)$ . To establish a baseline, we contrast this matched similarity against the similarity computed using randomly shuffled operand embeddings. We find that the matched similarity is very close to 1 and much higher than the randomly shuffled cosine similarity, suggesting that the MLP essentially takes the vector  $OV_2(a) + OV_2(b)$  as its input, regardless of the specific sequence.

**OV-MLP performs modular addition.** To verify the MLP’s active involvement in the addition circuit, we evaluate linear probes trained on the model’s internal activations. While probes applied prior to the layer-2 MLP fail to predict the model’s output, post-MLP probes succeed. This contrast demonstrates that indeed the layer-2 MLP is critical to compute the modular addition. As a final validation, we evaluate the isolated circuit directly. Computing the exact subnetwork  $W_U(\text{MLP}_2(\text{OV}_2(a) + \text{OV}_2(b)))$  on all pairs of constants achieves a 99.94% accuracy, nearly perfectly recovering the full model’s performance on the modular addition dataset.

**Variable-number equivalence.** To verify that the model employs an identical circuit for both variable-assigned and pure constant addition, we analyze the residual stream vector immediately preceding the final layer MLP. We compute the cosine similarity between sequences that share the same underlying addition operation (e.g.,  $b = 3 + b = 4 =$  versus  $+ 3 4 =$ ) and compare this against sequences with mismatched operands. As shown in Figure 5a, the cosine similarity is very close to 1 and significantly higher for matched operand pairs than for mismatched pairs. This confirms that a shared computational mechanism handles both input formats.

**Emergence of Fourier features.** To determine whether our model converges to known modular addition circuitry [12], we analyze the neuron preactivations in the layer-2 MLP. Specifically, we test for the presence of Fourier features, predicting that the preactivations for operands  $n$  and  $m$  take the theoretical form  $h_k(n, m) = \cos\left(\frac{2\pi k}{N}n + \alpha_k\right) + \cos\left(\frac{2\pi k}{N}m + \beta_k\right)$ . We observe a near-perfect match between this theoretical prediction and our empirically learned preactivations (see Figure 11 in Appendix A), confirming the model relies on this established periodic mechanism.

## 5.2 Variable Assignment via Induction Head

In this section, we reverse engineer the variable assignment module of our transformer. We begin by examining the attention patterns in layer 1, shown in Figure 4. These patterns exhibit two key traits: the  $=$  token attends specifically to positions 13 and 14, and the constant tokens preceding the  $+$  token attend to the variable situated directly before them.

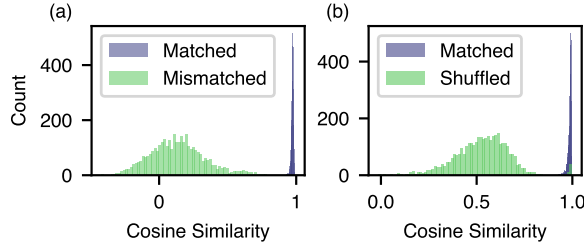


Figure 5: **Residual stream similarities.** (a) Cosine similarities between the pre-MLP residual stream vectors of different sequences. "Matched" pairs contain the same underlying addition operation (e.g.,  $b = 3 + b = 4 =$  versus  $+ 3 4 =$ ), whereas "Mismatched" pairs do not. The high similarity suggests that a shared representation handles both variable and constant formats. (b) Cosine similarity between the pre-MLP residual vector and the sum of the layer-2 output-value projections of the target operands,  $\text{OV}_2(a) + \text{OV}_2(b)$ . The high similarity compared to the randomly "Shuffled" baseline suggests that the modular addition operation is isolated to the  $QK_2$ -MLP circuit.

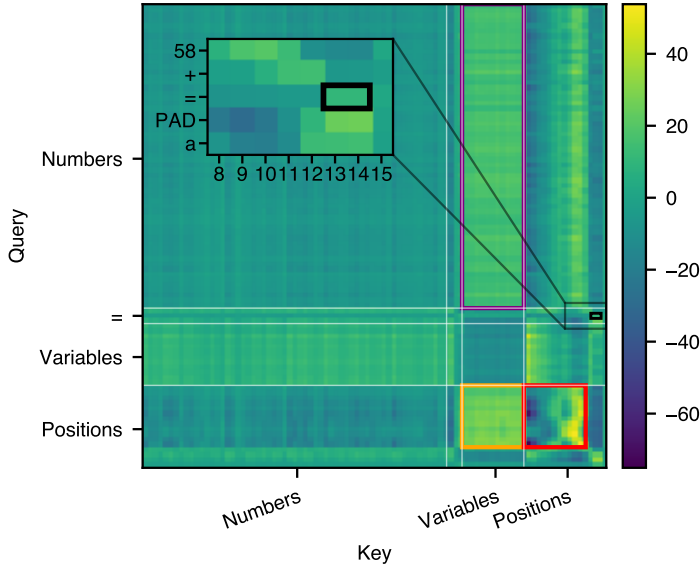


Figure 6: **Layer 1 QK matrix.** The previous-token head is formed by a combination of effects: constant tokens exhibit a strong preference for variables (purple outline); sequence positions 0–11, where variable assignments occur, also prefer variables (orange outline); and the positional interaction term generally increases toward the right (red outline). Furthermore, the  $=$  token attends specifically to the two preceding operand positions involved in the final addition (black outline).

To understand these behaviors, we analyze the layer 1  $QK$  matrix by testing it against all pairs of embeddings (Figure 6). We observe three distinct effects. First, the = token indeed exhibits a preference for the positional embeddings at 13 and 14 (black inset). Second, constant tokens interact strongly with variable tokens (purple outline), and positions 0–11—where the variable assignments occur—similarly attend to variables (orange outline). Third, the position-position attention term (red outline) generally increases towards the right.

Figure 7a analyzes this positional behavior in greater detail. Given the established preference for variables, we isolate the valid positions where a variable token can logically appear relative to a constant at position  $i$ . Specifically, we exclude positions greater than  $i$  (future tokens) due to causal masking and position  $i - 2$ , since the structural syntax dictates that a token two steps behind a constant must be either a PAD or another constant token. With these restrictions applied, Figure 7 reveals that constants in positions 0–11 possess a strict positional preference for the token immediately preceding them. This dynamic effectively acts as a previous-token head, ensuring constants attend directly to their assigned variables.

Consequently, after layer 1, the = token contains remapped embeddings  $OV_1(e_{\text{var}})$  of the variables in the addition in its residual stream, while the constant tokens in the assignments contained the remapped embeddings of the corresponding variables. Then, in the second layer attention, as Figure 7b demonstrates, the  $QK_2$  score between  $OV_1(e_{\text{var}_1})$  and  $OV_1(e_{\text{var}_2})$  is maximized strictly when  $\text{var}_1 = \text{var}_2$ . This confirms that the = token correctly attends to the specific constants associated with the variables used in the addition. By feeding these correct operands downstream, the attention mechanism directly enables the MLP to compute the final modular addition, successfully composing the two distinct operations.

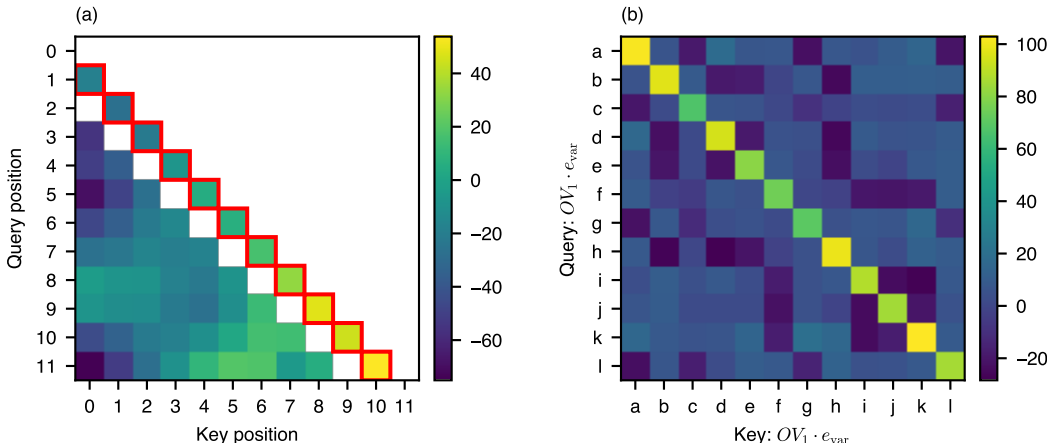


Figure 7: (a) **Layer 1 QK matrix on positional embeddings:** Causal masking is applied. The diagonals  $j = i$  and  $j = i - 2$  are excluded because a variable cannot appear in those positions relative to a constant at  $i$ . Red boxes indicate the maximum score in each row, demonstrating a strict preference for the immediately preceding position ( $j = i - 1$ ). (b) **Variable embedding similarity in Layer 2:** The transformation  $(OV_1E)QK_2(OV_1E)^\top$  exhibits a strong identity pattern. This demonstrates that tokens holding the same  $OV_1(e_{\text{var}})$  embedding will attend to one another.

## 6 Analyzing Training Dynamics with Progress Measures

In this section, we further analyze the different phases of training dynamics observed in Figure 2, by inspecting models at intermediate steps and implementing progress measures on specialized test sets in order to obtain a more fine-grained understanding. Recall that in the first phase (the first 5000 steps) the modular addition circuit is learned quickly before variable binding, although the latter begins to slowly emerge, as can be seen from the progress measures in Appendix B Figure 12. We now investigate the accuracy “spikes” around steps 5000 and 15000 in Figure 2.

The first spike occurs between steps 5300 and 5400 during the second phase of training, when the accuracy of the model on all non-var-restricted evaluation sets increases rapidly. Figure 8 shows that this transition coincides with the emergence of the variable-assignment routing circuit. Before the spike, the layer-1 attention

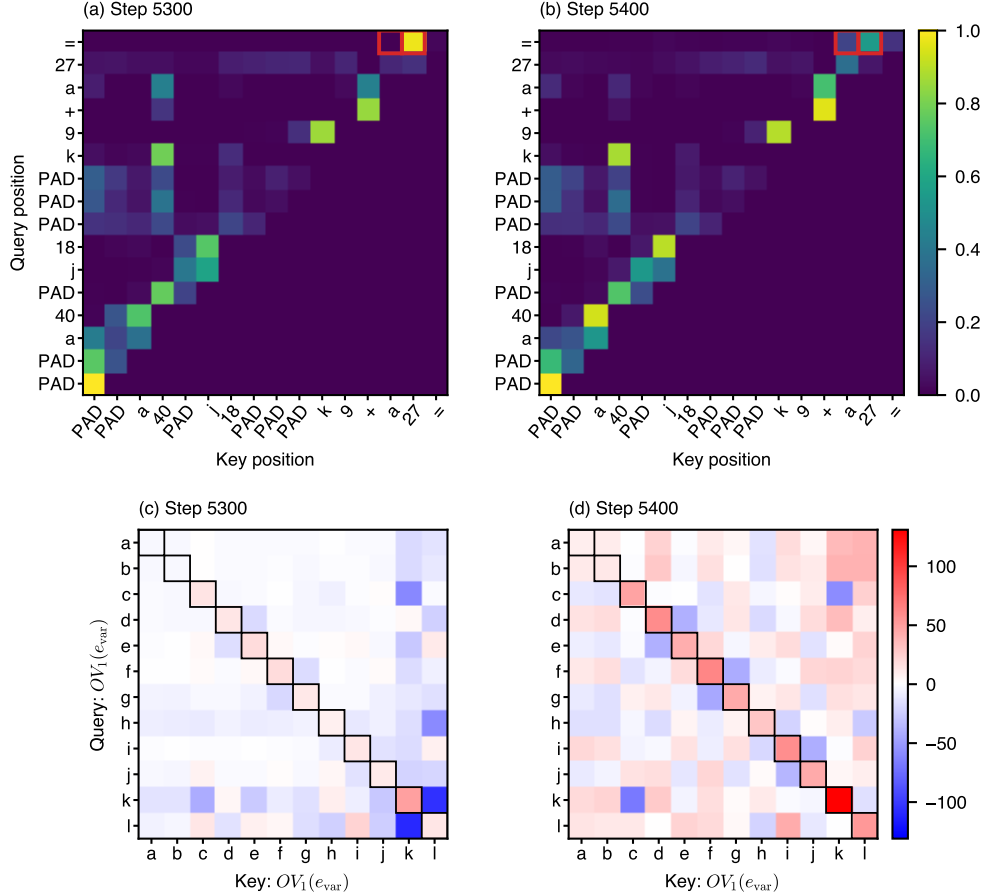


Figure 8: **Early emergence of variable assignment.** (a,b) Layer-1 attention patterns on a fixed 1-variable sequence immediately before and after the first accuracy spike. Red boxes mark the two operand positions that are queried by the = token in the final model. (c,d) The corresponding layer-2 QK scores on variables,  $(OV_1(e_{\text{var}}))QK_2(OV_1(e_{\text{var}}))^T$ . Across this transition, the variable-identity block becomes strongly diagonal, allowing the model to retrieve assigned constants.

pattern from the final = token still attends only to constant operands in 1-variable sequences, and the  $QK_2$  matrix is only weakly diagonal on variable embeddings. After the spike, the = token attends cleanly to the two operand positions, while the matrix  $(OV_1(e_{\text{var}}))QK_2(OV_1(e_{\text{var}}))^T$  develops the diagonal structure discussed in Section 5.2, producing the sharp increase in variable-containing accuracies.

The second spike, occurring between steps 14500 and 16000 in the final “refinement” phase of training, is more targeted: it brings the accuracy on var-restricted test sets in line with the rest. The failure of the model to generalize to var-restricted sequences before step 14500 is due to the model’s failure to correctly route sequences with b as the second operand, which are held out from the training set. This has two connected causes: the = token attends less strongly to b than it does to other variables in the first layer (Figure 9c), and the = token fails to attend to the variable-assigned constant in layer 2 when b is the second operand in a sequence (Figure 9d). As the  $QK_1$  scores for b improve, the  $QK_2$  scores and the accuracies for sequences with b as the second operand similarly improve.

## 7 Theoretical Insights on Training Dynamics

To further shed light on how the transformer learns to compose variable binding and modular addition, we now provide theoretical insights on how gradient dynamics can lead to such emergent compositionality, in a simplified model. We focus on the training of the second layer attention on one-variable data after the model has already learned the zero-variable modular addition mechanism, since the latter has already been

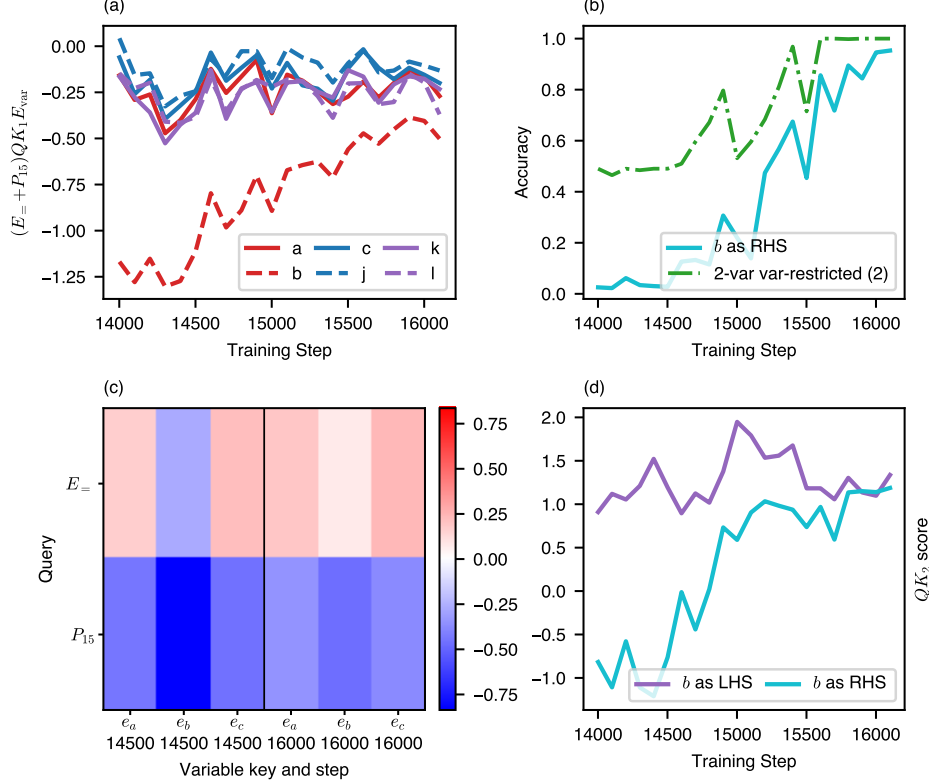


Figure 9: **Late correction of var-restricted routing.** (a) Variable-token contributions to the layer-1 attention from the = token, shown for selected variables. The **b** contribution begins substantially below the others and rises by the end of the window. (b) Accuracy on two-variable examples with **b** as the right operand, together with the fully var-restricted two-variable accuracy. The model completely fails to handle sequences with **b** as the right operand at the beginning of the window. (c) The projected variable-key matrix  $[E_{=}; P_{15}]QK_1 E_{\text{var}}^T$  for  $e_a, e_b, e_c$  at steps 14500 and 16000. (d) A component of the  $QK_2$  score between the tokens = and 7,  $\sum_{p=13}^{14} a_{=,p}^{(1)} a_{4,3}^{(1)} ((E_{x_p} + E_p)OV_1)QK_2(E_b OV_1)^T$  for the sequences PAD PAD **b** 7  $\dots$  + **b**/9 9/**b** = where  $a_{=,p}^{(1)}$  denotes the  $QK_1$  score from = to token at position  $p$  (either **b** or 9, and  $a_{4,3}^{(1)}$  denotes the  $QK_1$  score from 7 to **b**.

thoroughly studied in previous works [e.g., 13, 26, 27, 34].

Specifically, we consider a “disentangled” transformer [7, 9, 35] setup where all embeddings are normal and value-output matrices remap embeddings to new orthogonal subspaces. We denote by  $e_n$  for  $n \in \mathcal{N}$  the number embeddings,  $e_v$  for  $v \in \mathcal{V}$  the variable embeddings, and  $p_t$  for  $t \in [T]$  the positional embeddings, and consider “merged” key-query and output-value matrices  $W_{KQ}^\ell$  and  $W_{OV}^\ell$  at layer  $\ell = 1, 2$ . We assume the first layer attention as well as the modular addition MLP are already in place, while the second layer key-query matrix initially only attends to operand positions. We show that training this key-query matrix on one-variable data then leads to the relevant associative memory block which enables composition of variable assignment with modular addition.

**Theorem 7.1** (Informal). *In a simplified setup, the negative 1-variable population gradient w.r.t.  $W_{KQ}^2$  at  $\bar{W}_{KQ}^2 = \beta(p_{T-2} + p_{T-1})p_T^T + \beta \sum_{n \in \mathcal{N}} e_n p_T^T$ , with large enough  $\beta$ , has the following associative memory as its dominant term when  $N, T \gg V$ :  $\sum_{v \in \mathcal{V}} W_{OV}^1 e_v (W_{OV}^1 e_v + p_T)^T$ .*

Details are provided in Appendix C. Taking an update along this negative gradient direction with appropriate step-size then leads to the  $QK_2$  mechanism studied in Section 5, which enables composition of variable binding with modular addition. The initialization  $\bar{W}_{KQ}^2$  with large enough  $\beta$  ensures an initialization where the second layer attention focuses on the constants provided as operands, consistent with our experimental findings for the zero-variable mechanism. Our analysis shows that the key-query gradient is dominated by

terms involving the token with the correct assignment constant, thanks to a constructive interaction with the gradient of the MLP for the correct label.

## 8 Conclusion

In this work, we devise a mechanistically interpretable model for compositional generalization by considering a small transformer trained on a task that combines variable assignment and modular arithmetic. We demonstrate that the emergence of out-of-distribution generalization in training occurs via composition of independently-learned modular addition and variable assignment modules. The variable assignment is learned via a modified induction head circuit which we mathematically analyze, while modular addition follows the known Fourier circuit in the second-layer MLP. These results provide a mechanistic basis for understanding compositional generalization in more general mathematical reasoning problems.

Although our study provides several insights into compositional generalization through mechanistic analysis in a controlled setting, we only consider a task and model of limited complexity in order to ease analysis. We hope it can nonetheless motivate future investigations that may consider richer and more complex tasks, as well as more detailed and quantitative analysis which could lead further insight, e.g., on sample complexity or scaling considerations.

## References

- [1] Brenden M. Lake and Marco Baroni. Generalization without systematicity: On the compositional skills of sequence-to-sequence recurrent networks. In *International Conference on Machine Learning (ICML)*, 2018.
- [2] Najoung Kim and Tal Linzen. COGS: A compositional generalization challenge based on semantic interpretation. In *Conference on Empirical Methods in Natural Language Processing (EMNLP)*, 2020.
- [3] Ofir Press, Muru Zhang, Sewon Min, Ludwig Schmidt, Noah A. Smith, and Mike Lewis. Measuring and narrowing the compositionality gap in language models. In *Findings of the Association for Computational Linguistics (EMNLP)*, 2023.
- [4] Nouha Dziri, Ximing Lu, Melanie Sclar, Xiang Lorraine Li, Liwei Jiang, Bill Yuchen Lin, Sean Welleck, Peter West, Chandra Bhagavatula, Ronan Le Bras, Jena D. Hwang, Soumya Sanyal, Xiang Ren, Allyson Ettinger, Zaïd Harchaoui, and Yejin Choi. Faith and fate: Limits of transformers on compositionality. In *Advances in Neural Information Processing Systems (NeurIPS)*, 2023.
- [5] Nelson Elhage, Neel Nanda, Catherine Olsson, Tom Henighan, Nicholas Joseph, Ben Mann, Amanda Askell, Yuntao Bai, Anna Chen, Tom Conerly, Nova DasSarma, Dawn Drain, Deep Ganguli, Zac Hatfield-Dodds, Danny Hernandez, Andy Jones, Jackson Kernion, Liane Lovitt, Kamal Ndousse, Dario Amodei, Tom Brown, Jack Clark, Jared Kaplan, Sam McCandlish, and Chris Olah. A mathematical framework for transformer circuits. *Transformer Circuits Thread*, 2021.
- [6] Catherine Olsson, Nelson Elhage, Neel Nanda, Nicholas Joseph, Nova DasSarma, Tom Henighan, Ben Mann, Amanda Askell, Yuntao Bai, Anna Chen, Tom Conerly, Dawn Drain, Deep Ganguli, Zac Hatfield-Dodds, Danny Hernandez, Scott Johnston, Andy Jones, Jackson Kernion, Liane Lovitt, Kamal Ndousse, Dario Amodei, Tom Brown, Jack Clark, Jared Kaplan, Sam McCandlish, and Chris Olah. In-context learning and induction heads. *Transformer Circuits Thread*, 2022.
- [7] Alberto Bietti, Vivien Cabannes, Diane Bouchacourt, Hervé Jégou, and Léon Bottou. Birth of a transformer: A memory viewpoint. In *Advances in Neural Information Processing Systems (NeurIPS)*, 2023.
- [8] Gautam Reddy. The mechanistic basis of data dependence and abrupt learning in an in-context classification task. In *International Conference on Learning Representations (ICLR)*, 2024.

- [9] Eshaan Nichani, Alex Damian, and Jason D. Lee. How transformers learn causal structure with gradient descent. In *International Conference on Machine Learning (ICML)*, 2024.
- [10] Alethea Power, Yuri Burda, Harri Edwards, Igor Babuschkin, and Vedant Misra. Grokking: Generalization beyond overfitting on small algorithmic datasets, 2022.
- [11] Neel Nanda, Lawrence Chan, Tom Lieberum, Jess Smith, and Jacob Steinhardt. Progress measures for grokking via mechanistic interpretability. In *International Conference on Learning Representations (ICLR)*, 2023.
- [12] Andrey Gromov. Grokking modular arithmetic, 2023.
- [13] Jianliang He, Leda Wang, Siyu Chen, and Zhuoran Yang. On the mechanism and dynamics of modular addition: Fourier features, lottery ticket, and grokking, 2026.
- [14] Kevin Ro Wang, Alexandre Variengien, Arthur Conmy, Buck Shlegeris, and Jacob Steinhardt. Interpretability in the wild: a circuit for indirect object identification in GPT-2 small. In *International Conference on Learning Representations (ICLR)*, 2023.
- [15] Michael Hanna, Ollie Liu, and Alexandre Variengien. How does GPT-2 compute greater-than?: Interpreting mathematical abilities in a pre-trained language model. In *Advances in Neural Information Processing Systems (NeurIPS)*, 2023.
- [16] Emmanuel Ameisen, Jack Lindsey, Adam Pearce, Wes Gurnee, Nicholas L Turner, Brian Chen, Craig Citro, David Abrahams, Shan Carter, Basil Hosmer, et al. Circuit tracing: Revealing computational graphs in language models. *Transformer Circuits Thread*, 6:16318–16352, 2025.
- [17] Yi Zhang, Arturs Backurs, Sébastien Bubeck, Ronen Eldan, Suriya Gunasekar, and Tal Wagner. Unveiling transformers with lego: a synthetic reasoning task. *arXiv preprint arXiv:2206.04301*, 2022.
- [18] Bingbin Liu, Jordan T Ash, Surbhi Goel, Akshay Krishnamurthy, and Cyril Zhang. Transformers learn shortcuts to automata. In *International Conference on Learning Representations (ICLR)*, 2023.
- [19] Xander Davies, Max Nadeau, Nikhil Prakash, Tamar Rott Shaham, and David Bau. Discovering variable binding circuitry with desiderata. ICML 2023 Workshop on Deployable Generative AI, 2023.
- [20] Rahul Ramesh, Ekdeep Singh Lubana, Mikail Khona, Robert P. Dick, and Hidenori Tanaka. Compositional capabilities of autoregressive transformers: A study on synthetic, interpretable tasks. In *International Conference on Machine Learning (ICML)*, 2024.
- [21] Tianyu He, Darshil Doshi, Aritra Das, and Andrey Gromov. Learning to grok: Emergence of in-context learning and skill composition in modular arithmetic tasks. In *Advances in Neural Information Processing Systems (NeurIPS)*, 2024.
- [22] Yiwei Wu, Atticus Geiger, and Raphaël Milliere. How do transformers learn variable binding in symbolic programs? *arXiv preprint arXiv:2505.20896*, 2025.
- [23] Xingyu Zhao, Darsh Sharma, Rheeya Uppaal, and Yiqiao Zhong. Shattered compositionality: Counter-intuitive learning dynamics of transformers for arithmetic, 2026.
- [24] Johannes von Oswald, Eyvind Niklasson, Ettore Randazzo, João Sacramento, Alexander Mordvintsev, Andrey Zhmoginov, and Max Vladymyrov. Transformers learn in-context by gradient descent. In *International Conference on Machine Learning, (ICML)*, 2023.
- [25] Vivien Cabannes, Charles Arnal, Wassim Bouaziz, Xingyu Yang, François Charton, and Julia Kempe. Iteration head: A mechanistic study of chain-of-thought. In *Advances in Neural Information Processing Systems (NeurIPS)*, 2024.
- [26] Yuandong Tian. Composing global solutions to reasoning tasks via algebraic objects in neural nets, 2025.

- [27] Daniel Kunin, Giovanni Luca Marchetti, Feng Chen, Dhruva Karkada, James B Simon, Michael R DeWeese, Surya Ganguli, and Nina Miolane. Alternating gradient flows: A theory of feature learning in two-layer neural networks. In *Advances in Neural Information Processing Systems (NeurIPS)*, 2026.
- [28] Zixuan Wang, Eshaan Nichani, Alberto Bietti, Alex Damian, Daniel Hsu, Jason D. Lee, and Denny Wu. Learning compositional functions with transformers from easy-to-hard data. In *Annual Conference on Learning Theory (COLT)*, 2025.
- [29] Ashish Vaswani, Noam Shazeer, Niki Parmar, Jakob Uszkoreit, Llion Jones, Aidan N. Gomez, Lukasz Kaiser, and Illia Polosukhin. Attention is all you need. In *Advances in Neural Information Processing Systems (NeurIPS)*, 2017.
- [30] Guy Dar, Mor Geva, Ankit Gupta, and Jonathan Berant. Analyzing transformers in embedding space. In *Findings of the Association for Computational Linguistics (ACL)*, 2023.
- [31] Alec Radford, Jeffrey Wu, Rewon Child, David Luan, Dario Amodei, and Ilya Sutskever. Language models are unsupervised multitask learners. Technical report, OpenAI, 2019.
- [32] Neel Nanda and Joseph Bloom. Transformerlens. <https://github.com/TransformerLensOrg/TransformerLens>, 2022.
- [33] Ilya Loshchilov and Frank Hutter. Decoupled weight decay regularization. In *International Conference on Learning Representations (ICLR)*, 2019.
- [34] Depen Morwani, Benjamin L. Edelman, Costin-Andrei Oncescu, Rosie Zhao, and Sham M. Kakade. Feature emergence via margin maximization: case studies in algebraic tasks. In *International Conference on Learning Representations (ICLR)*, 2024.
- [35] Dan Friedman, Alexander Wettig, and Danqi Chen. Learning transformer programs. In *Advances in Neural Information Processing Systems (NeurIPS)*, 2023.

## A Additional Experimental Results

Figure 10 shows the accuracies by evaluation set for another training run with the same parameters. The same “spikes” in non-var-restricted and var-restricted accuracies seen in Figure 2 are also displayed here, although at different times.

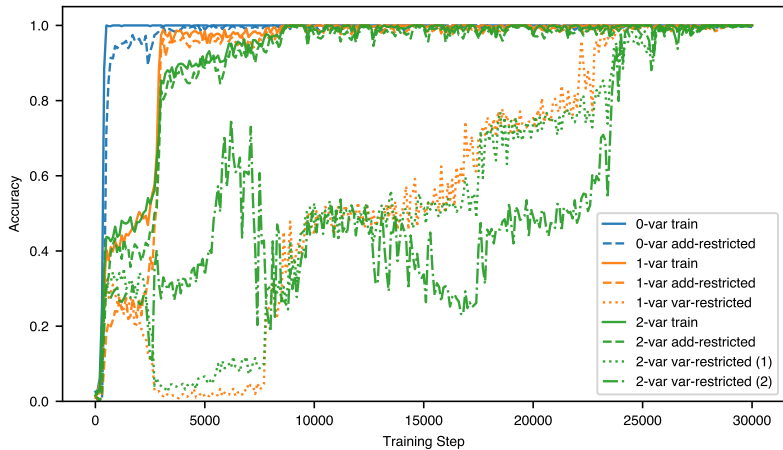


Figure 10: **Accuracies for alternate initialization.** For completeness, we recreate Figure 2 for another training run. In this training run, the lowered  $b$  accuracy discussed in Section 6 instead appears for sequences with  $k$  on the left-hand side.

Figure 11 displays the preactivations for neuron 70 (left) and the preactivations for the theoretical construction of an MLP trained to perform modular addition in Gromov [12]. The figure shows a near-perfect match, suggesting our model indeed implements the same MLP circuit that has been previously discovered in the literature.

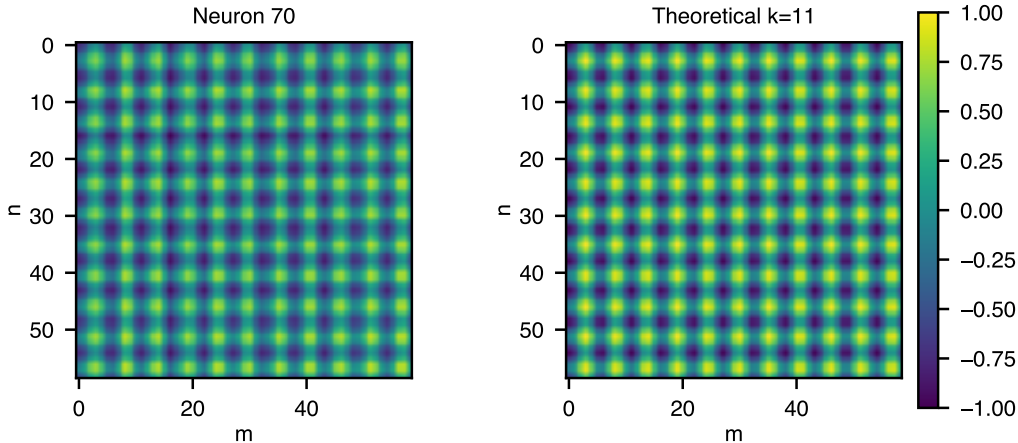


Figure 11: **Emergence of Fourier features in the layer-2 MLP.** The learned preactivations of a specific neuron (Neuron 70) across all operand pairs  $(n, m)$ . match the corresponding theoretical 2D Fourier feature for frequency  $k = 11$  predicted by Gromov [12].

## B Progress Measures

We implement a variety of progress measures to track training dynamics:

- **ov2\_mlp2\_accuracy:** Tracks the accuracy of  $W_U(MLP_2(OV_2(a) + OV_2(b)))$  over all  $59^2$  addition pairs
- **qk1\_num\_to\_prev\_var:** A memory probe that tracks whether the  $QK_1$  score for positional  $\times$  positional embeddings is maximized when  $j = i - 1$ .
- **qk2\_ov1\_var\_identity:** Tracks whether  $(OV_1(E))QK_2(OV_1(E))^T$  for variable embeddings is the identity.
- **attn\_l1\_equal\_to\_operands:** Tracks whether, for a batch of sequences, the = token attends to the operands of the addition in layer 1.
- **attn\_l1\_num\_to\_prev:** Tracks whether, for a batch of sequences, the number tokens in positions 1 – 11 attend to the previous (variable) token in layer 1.
- **attn\_l2\_equal\_to\_values:** Tracks whether, for a batch of sequences, the = token attends to the correct constants in layer 1.
- **probe\_l1\_var\_from\_num:** Tracks whether, for a batch of sequences, a linear probe can be trained to classify the corresponding variable name from the residual stream vector on the number tokens after the layer 1 attention.

These progress measures reveal the order in which the model learns different elements of the circuit in training. In particular, training can be divided into three phases. In the first phase, `ov2_mlp2_accuracy` rises sharply, indicating that the final-layer MLP implements modular addition once the correct operands are provided. This coincides with the model achieving 100% accuracy on 0-variable sequences by the end. Furthermore, towards the end of this phase, we see the emergence of a variable binding mechanism with measures that track variable binding, such as `probe_l1_mid_var_from_num`, reaching 80%.

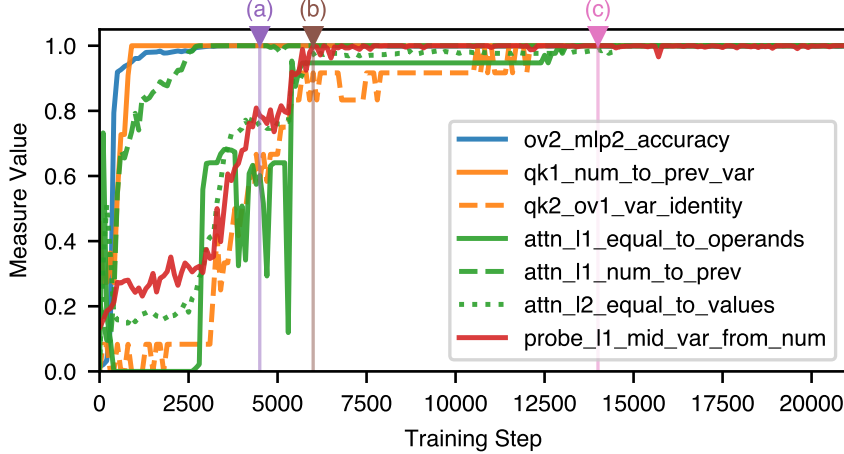


Figure 12: (a) End of the first phase of training, characterized by generalization on 0-variable addition and the emergence of structure for variable assignment. (b) End of the second phase of training, characterized by the rapid development of the variable assignment circuit (c) End of the last phase of training, characterized by the model “cleaning up” the variable assignment module and generalizing on all evaluation sets.

In the second phase, the model rapidly learns to bind variables to their assigned constants, corresponding to the first “spike” discussed in Section 6. This is evidenced by `probe_l0_var_from_num` reaching 100%, indicating that variable names are successfully copied into the constant tokens’ residual streams. However, the metrics tracking the routing between the assignment module and the addition module (`qk1_ov0_var_identity`, `attn_l0_equal_to_operands`, and `attn_l1_equal_to_values`) plateau between 80% and 99%, corresponding to the model not yet being able to correct route constants assigned to `b` (Section 6).

In the final phase, the model bridges the remaining performance gap by , achieving > 99% accuracy across all benchmarks, including the var-restricted sets. This ordering confirms that the model first masters the core modular addition operation, and subsequently learns to generalize by correctly routing the assigned variables into this established circuit.

## C Theoretical Analysis of Gradient Dynamics

**Architecture.** To simplify our analysis, we assume that the first layer mechanisms are already in place, by considering a single layer of attention on top of augmented inputs of the form:

$$\begin{aligned}
 x_t &= \begin{cases} p_t + e_{n_t} + \Phi_1 e_{v_t}, & \text{if } t \in \tau \\ p_t + e_{pad}, & \text{if } t \in [T-3] \setminus \tau, \end{cases} \\
 x_{T-2} &= p_{T-2} + e_{v^*} \\
 x_{T-1} &= p_{T-1} + e_m \\
 x_T &= p_T + \Phi_1 e_{v^*}.
 \end{aligned} \tag{1}$$

In this example, the operands are the number  $m \in \mathcal{N}$  and the variable  $v^* \in \mathcal{V}$ , while the assignments are  $(v_t, n_t) \in \mathcal{V} \times \mathcal{N}$  for  $t \in \tau \subset [T-3]$ , meaning that they appear at positions  $t \in \tau$ , while other positions are just pad tokens, and we assume  $v^* \in \{v_t\}_{t \in \tau}$ . The matrix  $\Phi_1$  mimicks the value matrix  $W_{OV}^1$ , and we assume here that it maps embeddings to a new orthogonal subspace, similar to a random matrix in high dimensions, as in [7].

The architecture we consider then is a single attention layer with an MLP on top:

$$F_\alpha(x_{1:T}) = \alpha M(\Phi_2 X \sigma(X^\top W x_T)), \tag{2}$$

where  $X = [x_1 \cdots x_T] \in \mathbb{R}^{d \times T}$ ,  $W$  denotes the key-query matrix,  $\Phi_2$  the value-output matrix,  $\sigma$  the attention softmax, and  $M(\cdot)$  the MLP which maps  $d$ -dimensional representations  $x$  to unscaled logits  $M_k(x)$  for each

vocabulary element  $k \in \mathcal{N}$ . The scalar  $\alpha > 0$  controls the initial scale of the final logits; the proof below considers the small-output regime  $\alpha \ll 1$ , after which  $\alpha$  may be increased to sharpen predictions without changing the direction of the key-query signal analyzed here. We assume  $\Phi_2$  is a fixed remapping to a new orthogonal subspace, and  $M$  follows the construction in [12, Appendix A] with complex-valued weights:

$$M_k(x) = \frac{1}{N} \sum_{j=1}^N u_{k,j} (v_j^\top x)^2, \text{ with}$$

$$v_j = \sum_{n=1}^N e^{2i\pi \frac{jn}{N}} \Phi_2 e_n, \quad \text{and} \quad u_{k,j} = e^{-2i\pi \frac{jk}{N}}.$$

This implies  $M_k(\Phi_2 e_n + \Phi_2 e_m) = 2 \cdot \mathbf{1}\{k = n + m\} + \mathbf{1}\{k = 2n\} + \mathbf{1}\{k = 2m\}$ , where equalities are intended as modulo  $N$ . We also note that we have  $\nabla M_k(\Phi_2 e_n)^\top \Phi_2 e_m = 2 \cdot \mathbf{1}\{k = n + m\}$ , a property which will be useful in our gradient analysis.

**Gradient dynamics.** We assume the model is initialized at

$$W_0 = \beta(p_{T-2} + p_{T-1})p_T^\top + \beta \sum_{n \in \mathcal{N}} e_n p_T^\top, \quad (3)$$

which leads to an attention behavior similar to that observed in Figure 8(a) when  $\beta$  is chosen appropriately, and analyze the behavior when taking gradient steps on one-variable data.

We consider a data distribution  $p$  over sequence-label pairs  $(x_{1:T}, y)$  that are generated as follows:  $x_{1:T}$  is a one-variable sequence of the form (1), where we assume  $\tau = \{t^*\}$ , with  $t^* \sim \text{Unif}([T-3])$ , with an assignment variable  $v \sim \text{Unif}(\mathcal{V})$ , assigned number and second operand  $n, m \sim \text{Unif}(\mathcal{N})$ . The label is  $y = n + m \pmod N$ . The loss takes the form

$$L(W) = \mathbb{E}_{(x,y) \sim p} [\ell(y, F_\alpha(x_{1:T}))], \quad (4)$$

where  $\ell(y, \xi) = -\xi_y + \log \sum_k \exp(\xi_k)$  is the cross-entropy loss and  $F_\alpha$  is defined in (2).

**Theorem C.1** (One gradient step leads to composition). *Consider the population loss (4) over the data distribution  $p$  defined above, and the initialization  $W_0$  in (3). Let  $\sigma = \sigma(X^\top W_0 x_T)$  and assume that  $\beta$  is large enough so that  $\sigma_{T-1} = \rho_1 = \Theta(1)^1$  while  $\rho_2 := \sigma_{t^*} = \Theta(1/T)$ , and  $\sigma_t = \Theta(1/T)$  for all  $t \neq T-1$ . Consider one gradient step  $W_1 = W_0 - \eta \nabla L(W_0)$  with learning rate*

$$\eta = \frac{VN}{2\alpha\rho_1\rho_2(N-1)}.$$

Then

$$W_1 = \tilde{W}_0 + \sum_{v \in \mathcal{V}} \Phi_1 e_v (\Phi_1 e_v + p_T)^\top + O_\infty \left( V \left( \frac{1}{N} + \frac{1}{T} + T\alpha \right) \right),$$

where the  $O_\infty(\cdot)$  term is in matrix infinity norm in the orthogonal embedding basis, and where we define  $\tilde{W}_0 := W_0 - (2\rho_1 - 1)p_{T-1}(Vp_T^\top + \sum_{v \in \mathcal{V}} (\Phi_1 e_v)^\top)$  as the initial matrix with an additional term, which attenuates the pre-existing attraction to position  $T-1$  when  $\rho_1 > 1/2$ . Note that when  $N, T \gg V$  and the final-logit scale  $\alpha$  is small enough that  $VT\alpha \ll 1$ , the displayed associative-memory term dominates the update.

The associative-memory term in  $W_1$  is sufficient to ensure attention to the correct variables in the context, even when  $\tau$  has more than one variable. Note that the component  $\sum_v \Phi_1 e_v p_T^\top$  also gives some attention to all assignments, but with lower scores, and this spurious term should be attenuated if one takes subsequent steps on data involving more variables in  $\tau$ .

The small-output scale condition above is a standard way of replacing the idealization  $\hat{p}(k|x_{1:T}) = 1/N$  by a perturbative argument: at small final-logit scale the prediction softmax remains close to uniform, and the non-uniformity contributes only a controlled remainder. Similar small-initialization arguments appear in theoretical analyses of transformer training dynamics [e.g., 9, 28].

<sup>1</sup>Remark that  $\sigma_{T-1}$  is independent of the inputs for this specific data model considered, under orthogonal embeddings.

*Proof.* Let  $\varepsilon_\alpha = e^{2\alpha} - 1$ . The gradient at  $W = W_0$  is then given by

$$\nabla L = \alpha \sum_{k \in \mathcal{N}} \mathbb{E} \left[ \left( \hat{p}_\alpha(k|x_{1:T}) - \mathbf{1}\{y = k\} \right) \sum_t \sigma_t \nabla M_k(z)^\top \Phi_2 x_t \cdot (x_t - \bar{x}_{1:T}) x_T^\top \right],$$

where we define  $\sigma_t = \sigma(X^\top W_0 x_T)_t$ ,  $z = \Phi_2 X \sigma$ , and  $\bar{x}_{1:T} = \sum_t \sigma_t x_t$ , and  $\hat{p}_\alpha(k|x_{1:T}) = \text{softmax}(\alpha M(z))_k$  denotes the prediction of the current model. We first bound the unscaled logits  $M(z)$ . Under the orthogonality assumptions on  $\Phi_2$ , the Fourier vectors  $v_j$  only overlap with the number-embedding components of the input, and are orthogonal to all other embeddings, so that we have  $|v_j^\top \Phi_2 x_t| \leq 1$ , with equality only possible at positions with a number component. Therefore, for every  $j$ ,

$$|v_j^\top z| = \left| \sum_t \sigma_t v_j^\top \Phi_2 x_t \right| \leq \sum_t \sigma_t = 1,$$

and, since  $|u_{k,j}| = 1$ ,

$$|M_k(z)| \leq \frac{1}{N} \sum_{j=1}^N |v_j^\top z|^2 \leq 1.$$

Hence, for every  $k$  we have

$$\begin{aligned} \frac{e^{-2\alpha}}{N} \leq \hat{p}_\alpha(k|x_{1:T}) \leq \frac{e^{2\alpha}}{N}, \quad \hat{p}_\alpha(k|x_{1:T}) &= \frac{1}{N} + r_k(x_{1:T}), \\ |r_k(x_{1:T})| &\leq \frac{\varepsilon_\alpha}{N}. \end{aligned}$$

Thus the gradient can be decomposed as  $\nabla L = \alpha(\nabla L_{\text{unif}} + R_\alpha)$ , where

$$\begin{aligned} \nabla L_{\text{unif}} &= \sum_{k \in \mathcal{N}} \mathbb{E} \left[ \left( \frac{1}{N} - \mathbf{1}\{y = k\} \right) A_k(x_{1:T}) \right], \\ R_\alpha &= \sum_{k \in \mathcal{N}} \mathbb{E} [r_k(x_{1:T}) A_k(x_{1:T})], \end{aligned}$$

with

$$A_k(x_{1:T}) = \sum_t \sigma_t \nabla M_k(z)^\top \Phi_2 x_t \cdot (x_t - \bar{x}_{1:T}) x_T^\top.$$

The matrices  $A_k(x_{1:T})$  have uniformly  $O(1)$  entries: indeed, the bounds above imply

$$|\nabla M_k(z)^\top \Phi_2 x_t| = \left| \frac{2}{N} \sum_j u_{k,j} (v_j^\top z) (v_j^\top \Phi_2 x_t) \right| \leq 2,$$

while  $\sum_t \sigma_t = 1$ , and the vectors  $x_t$ ,  $\bar{x}_{1:T}$ , and  $x_T$  have  $O(1)$  coordinates in the orthogonal embedding basis. Hence, using  $|r_k(x_{1:T})| \leq \varepsilon_\alpha/N$ ,

$$\|R_\alpha\|_\infty \leq \sum_{k \in \mathcal{N}} \mathbb{E} [\|r_k(x_{1:T})\| \|A_k(x_{1:T})\|_\infty] \leq C\varepsilon_\alpha = O(\alpha)$$

for small  $\alpha$  and a universal constant  $C$ . Thus  $\nabla L = \alpha(\nabla L_{\text{unif}} + O_\infty(\varepsilon_\alpha))$ , so the perturbation from the non-uniform prediction softmax is negligible as  $\alpha \rightarrow 0$ .

Expanding the gradient  $\nabla M_k$ , we have

$$\begin{aligned} \nabla M_k(z)^\top \Phi_2 x_t &= \frac{2}{N} \sum_j u_{k,j} (v_j^\top z) (v_j^\top \Phi_2 x_t) \\ &= \frac{2}{N} \sum_{t'} \sigma_{t'} \sum_j u_{k,j} (v_j^\top \Phi_2 x_t) (v_j^\top \Phi_2 x_{t'}). \end{aligned}$$

We also denote  $\rho_2 = \sigma_{t^*} = \Theta(1/T)$ , which is independent of the specific sequence under our assumptions of  $W_0$ .

We may write

$$\begin{aligned} A_k(x_{1:T}) &= \frac{2}{N} \sum_{t,t'} \sigma_t \sigma_{t'} \sum_j u_{k,j} (v_j^\top \Phi_2 x_t) (v_j^\top \Phi_2 x_{t'}) \\ &\quad \cdot (x_t - \bar{x}_{1:T}) x_T^\top \\ &= 2\rho_1^2 \delta_{k,m,m} (x_{T-1} - \bar{x}_{1:T}) x_T^\top \\ &\quad + 2\rho_2^2 \delta_{k,n,n} (x_{t^*} - \bar{x}_{1:T}) x_T^\top \\ &\quad + 2\rho_1 \rho_2 \delta_{k,m,n} (x_{t^*} + x_{T-1} - 2\bar{x}_{1:T}) x_T^\top, \end{aligned}$$

with  $\delta_{k,m,n} = \frac{1}{N} \sum_j u_{k,j} (v_j^\top \Phi_2 e_n) (v_j^\top \Phi_2 e_m) = \mathbf{1}\{k = m + n\}$ , by noting that  $v_j^\top \Phi_2 x_t = 0$  for  $t \notin \{t^*, T-1\}$ .

Based on the three terms above, the uniform part of the gradient satisfies

$$\nabla_W L_{\text{unif}} = G_1 + G_2 + G_3,$$

with (using that  $y = n + m$ )

$$\begin{aligned} G_1 &= 2\rho_1^2 \sum_{k \in \mathcal{N}} \mathbb{E}[(\frac{1}{N} - \mathbf{1}\{n + m = k\}) \mathbf{1}\{k = 2m\} (x_{T-1} - \bar{x}_{1:T}) x_T^\top] \\ &= 2\rho_1^2 \mathbb{E}[(\frac{1}{N} - \mathbf{1}\{n = m\}) (x_{T-1} - \bar{x}_{1:T}) x_T^\top] \\ &= 0, \end{aligned}$$

by noting that  $x_T$  is independent of  $n$  and  $m$ , while each  $x_t$ ,  $t < T$  only depends on either  $m$  or  $n$  (or neither), so that  $\mathbb{E}_{m,n}[\mathbf{1}\{m = n\} x_t | v] = \frac{1}{N} \mathbb{E}[x_t | v]$ . Similarly,

$$\begin{aligned} G_2 &= 2\rho_2^2 \sum_{k \in \mathcal{N}} \mathbb{E}[(\frac{1}{N} - \mathbf{1}\{n + m = k\}) \mathbf{1}\{k = 2n\} (x_{t^*} - \bar{x}_{1:T}) x_T^\top] \\ &= 2\rho_2^2 \mathbb{E}[(\frac{1}{N} - \mathbf{1}\{n = m\}) (x_{t^*} - \bar{x}_{1:T}) x_T^\top] \\ &= 0. \end{aligned}$$

Finally, the last term contains the signal, as follows:

$$\begin{aligned} G_3 &= 2\rho_1 \rho_2 \sum_{k \in \mathcal{N}} \mathbb{E}[(\frac{1}{N} - \mathbf{1}\{n + m = k\}) \mathbf{1}\{k = m + n\} (x_{t^*} + x_{T-1} - 2\bar{x}_{1:T}) x_T^\top] \\ &= -2\rho_1 \rho_2 \frac{N-1}{N} \mathbb{E}[(x_{t^*} + x_{T-1} - 2\bar{x}_{1:T}) x_T^\top] \\ &= -2\rho_1 \rho_2 \frac{N-1}{N} \mathbb{E}[(\Phi_1 e_v + e_n + p_{t^*} + (1-2\rho_1)(e_m + p_{T-1}) \\ &\quad - O(1/T)(e_n + e_m + e_v + \Phi_1 e_v + \sum_t p_t)) (\Phi_1 e_v + p_T)^\top] \\ &= -2\rho_1 \rho_2 \frac{N-1}{N} \left( \frac{1}{V} \sum_{v \in \mathcal{V}} \Phi_1 e_v (\Phi_1 e_v + p_T)^\top - (2\rho_1 - 1) p_{T-1} p_T^\top \right. \\ &\quad \left. - \frac{2\rho_1 - 1}{V} p_{T-1} \sum_v (\Phi_1 e_v)^\top + O_\infty \left( \frac{1}{N} + \frac{1}{T} \right) p_T^\top \right), \end{aligned}$$

where  $O_\infty(\epsilon)$  is a vector whose coordinates in the orthogonal basis of all embeddings are bounded by  $\epsilon$ . In particular, when  $N, T \gg V$ , the last term is negligible, in the sense that it has little effect on attention logits after the gradient update. The first term is the associative-memory term, while the second and third terms subtract away some of the attention to the second operand that is already present for the model at  $W_0$ .

Combining this display with  $\nabla L = \alpha(G_3 + O_\infty(\varepsilon_\alpha))$ , using  $\varepsilon_\alpha = O(\alpha)$  and  $(\rho_1\rho_2)^{-1} = O(T)$ , and taking

$$\eta = \frac{VN}{2\alpha\rho_1\rho_2(N-1)}$$

gives

$$\begin{aligned} W_1 &= W_0 - \eta\nabla L(W_0) \\ &= W_0 + \sum_{v \in \mathcal{V}} \Phi_1 e_v (\Phi_1 e_v + p_T)^\top - (2\rho_1 - 1)V p_{T-1} p_T^\top \\ &\quad - (2\rho_1 - 1)p_{T-1} \sum_{v \in \mathcal{V}} (\Phi_1 e_v)^\top + O_\infty \left( V \left( \frac{1}{N} + \frac{1}{T} + T\alpha \right) \right), \end{aligned}$$

where the final  $O_\infty(\cdot)$  is now interpreted in matrix infinity norm. This proves the claimed expression for the normalized one-step update. □